Biology of Reproduction, 2022, **107(2)**,406–418
https://doi.org/10.1093/biolre/ioac064
Advance access publication date 23 April 2022
Research Article

Dynamic zinc fluxes regulate meiotic progression in *Caenorhabditis elegans*†

Adelita D. Mendoza[1,2], Aaron Sue[1,2], Olga Antipova[3], Stefan Vogt[3], Teresa K. Woodruff[1,2,4,*], Sarah M. Wignall[1,*] and Thomas V. O'Halloran[1,2,5,6,*]

[1]Department of Molecular Biosciences, Northwestern University, Evanston, IL, USA
[2]The Chemistry of Life Processes Institute, Northwestern University, Evanston, IL, USA
[3]X-ray Science Division, Advanced Photon Source, Argonne National Laboratory, Argonne, IL, USA
[4]Department of Obstetrics and Gynecology, College of Human Medicine, Michigan State University, East Lansing, MI USA
[5]Department of Chemistry, Northwestern University, Evanston, IL, USA
[6]Department of Chemistry and Department of Microbiology and Molecular Genetics, Michigan State University, East Lansing, MI USA

***Correspondence**: Department of Chemistry and Department of Microbiology and Molecular Genetics, Michigan State University, Interdisciplinary Science and Technology Building Room 3022, 766 Service Rd., East Lansing, MI 48823, USA. Tel: 517-353-4090; Fax: 517-353-2446; E-mail: ohallor8@msu.edu; Department of Obstetrics, Gynecology and Reproductive Biology, Michigan State University, Interdisplinary Science and Technology Building Room 3006, 766 Service Rd. East Lansing, MI 48823, USA. Tel: 517-353-4090; Fax: 517-353-2446; E-mail: tkw@msu.edu and Department of Molecular Biosciences, Northwestern University, 2205 Tech Drive, Hogan 2-100, Evanston, IL 60208. E-mail: s-wignall@northwestern.edu

†**Grant support**: This project was supported by NIH grants R01GM115848 to TVO and TKW, R01GM038784, P41GM181350 to TVO, and R01GM124354 to SMW. ADM was supported by the Ruth L. Kirchenstein F31 NRSA (F31GM112478) and the Chicago Biomedical Consortium Scholarship (A2011-00985). Elemental analysis was performed at the Northwestern University Quantitative Bio-element Imaging Center supported by the Office of the Director, National Institutes of Health via NIH grants S10OD026786 and S10OD020118. Research at the Advanced Photon Source, a U.S. Department of Energy (DOE) Office of Science User Facility operated for the DOE Office of Science by Argonne National Laboratory was supported under Contract No. DE-AC02-06CH11357.

Abstract

Zinc influx and efflux events are essential for meiotic progression in oocytes of several mammalian and amphibian species, but it is less clear whether this evolutionary conservation of zinc signals is also important in late-stage germline development in invertebrates. Using quantitative, single cell elemental mapping methods, we find that *Caenorhabditis elegans* oocytes undergo significant stage-dependent fluctuations in total zinc content, rising by over sevenfold from Prophase I through the beginning of mitotic divisions in the embryo. Live imaging of the rapid cell cycle progression in *C. elegans* enables us to follow changes in labile zinc pools across meiosis and mitosis in single embryo. We find a dynamic increase in labile zinc prior to fertilization that then decreases from Anaphase II through pronuclear fusion and relocalizes to the eggshell. Disruption of these zinc fluxes blocks extrusion of the second polar body, leading to a range of mitotic defects. We conclude that spatial temporal zinc fluxes are necessary for meiotic progression in *C. elegans* and are a conserved feature of germ cell development in a broad cross section of metazoa.

Summary Sentence

Dynamic, large-scale zinc fluxes regulate events during meiotic progression in *C. elegans* embryos, including polar body extrusion and pronuclear migration.

Graphical Abstract

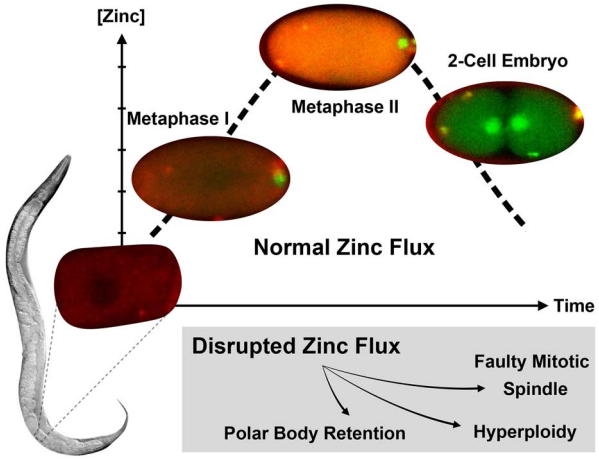

Keywords: C. elegans, oogenesis, egg activation, meiosis, zinc, X-ray fluorescence microscopy

Received: May 19, 2021. **Revised:** October 14, 2021. **Accepted:** March 20, 2022

Introduction

Cellular signaling pathways employ two types of canonical inorganic signal mediators; the phosphorelay systems depend upon covalent mechanisms [1], whereas calcium receptors employ compartmentalization and release of a diffusible ionic signal mediator to drive function [2]. Zinc is emerging as a third type of inorganic signal mediator and exhibits properties of both ionic and covalent signaling pathways. It is compartmentalized in a chemically labile form that can undergo triggered release, diffusion, and reuptake much like calcium transients, but, like phosphate, it can also form robust covalent bonds in allosteric sites of enzymes and transcription factors [3–5], and thereby trigger repression [6–8] or activation of gene expression [9–11]. Fluctuations in zinc activity were first shown to act as a signal regulating cell cycle progression using quantitative inorganic mapping methods to characterize meiotic maturation in mammalian oocytes [12]. Briefly, mammalian oocytes must take up a large bolus of zinc to pass through key checkpoints in the late stages of meiotic maturation [12]. Over a relatively short, 12-h, time period, mouse oocytes import over 20 billion zinc atoms from the extracellular space, representing a 50% increase in the total cellular zinc quota. Zinc uptake is essential for completion of meiosis I and blocking this inward zinc flux results in meiotic failure at telophase. Zinc influx during MI is also required for the transition from MI to MII independent of the Mos/mitogen-activated protein kinase pathway [13], and for CCNB1 and Maturation promoting factor (MPF) activity. The relationship between zinc and CCNB1 activity is likely exerted through zinc binding to the zinc-binding protein, EMI2, a cytostatic factor component [14]. At fertilization, the MII egg must exocytose zinc ions in a process known as "zinc sparks". This outward zinc flux is required for the egg-to-zygote transition and meiotic-to-mitotic cell cycles. Zinc uptake and exocytosis occur in mouse [12, 15, 16], rhesus macaque [15], crab-eating macaque [15], fly [17], frog [18], bovine, and humans [15, 19]. Pharmacological reduction of zinc availability via TPEN treatment in the MII-arrested egg promotes activation and reentry into the cell cycle and thus mimics the effects of the zinc spark events [15]. Likewise, reintroduction of zinc (via treatment with a zinc ionophore) after egg activation blocks the final stage of meiosis, leads to reversal to an MII-like stage of cell cycle arrest that includes reformation of the metaphase spindle and reestablishment of the actin cap [15]. The mediators, receptors, and targets of these transient zinc fluctuations vary depending on cell stage but include the zinc-specific transporters Zip6 and Zip10 [20] as well as glycoproteins in the zona pellucida (ZP) [16]. Although these quantitative elemental mapping studies have established zinc ions as biological signaling agents that regulate mammalian meiotic progression, it remains unclear whether such mechanisms are conserved in other metazoans.

The readily accessible and translucent reproductive tract of *Caenorhabditis elegans* enables interrogation of fluctuations in intracellular zinc in live cells across the transition from meiosis to mitosis including late egg development, fertilization, and early embryo formation. By applying ultratrace quantitative methods that are capable of detecting extremely small quantities of metals in submicron volumes, to single *C. elegans* cells at several stages in meiotic maturation and the egg-to-embryo transition, we establish that each stage has a distinct elemental signature that is best described as a quantitative inorganic phenotype. These experiments employ single cell X-ray fluorescence microscopy on air-dried cells to gauge the total zinc content in terms of atoms per cell [12, 15, 16, 20–24]. In addition, the fact that *C. elegans* undergoes rapid and well characterized progression through these stages allows us, for the first time in any organism, to continuously follow the dynamic fluctuations in zinc concentration at each stage in real time. Fluorescence microscopy of live embryos treated with zinc responsive dyes such as ZincBY−1 reveal changes in labile zinc, which is the fraction of the total cellular zinc that exists in exchangeable pools and is available to bind to a probe with a dissociation constant in the nanomolar range [15, 23]. We find that zinc influx in *C. elegans* oocytes begins after Prophase I and increased by ∼700% peaking just before mitosis; in comparison, mouse oocytes increase zinc content across these stages by only 50%. As the *C. elegans* embryo progressed from Anaphase II through pronuclear fusion, zinc was reallocated to the eggshell and, as is the case in mouse, total cellular zinc decreased as meiosis ended and mitosis in the fertilized embryo began. Severe defects in meiotic and mitotic progression occur if zinc uptake is blocked. Overall, these results establish quantitative inorganic phenotypes for discrete stages across the full meiotic and mitotic cell cycle progression for the first time in any organism. These zinc fluxes occurred at similar stages as those reported for mammalian oocytes. Thus, zinc signals are necessary for egg-to-embryo transitions in invertebrate reproduction and this work provides a foundation for future mechanistic studies of some of the earliest signaling biology in the life cycles of metazoa.

Materials and methods

Worm strains

EU1067 (*unc-119(ed3) ruIs32[unc-119(+)pie-1*^{promoter}*::GFP::H2B]III; ruIs57[unc-119(+)pie-1*^{promoter}*::GFP::tubulin]*) was used to visualize the meiotic spindle in the labile zinc fluorescence experiments [25]. N2 (Bristol) wild-type strain was used in oocyte maturation X-ray fluorescence microscopy (XFM) experiments. AV335 (*emb − 27(g48)II; unc-119(ed3) ruIs32[unc-119(+) pie-1*^{promoter}*::GFP::H2B]III; ruIs57[unc-119(+) pie-1*^{promoter}*::GFP::tubulin]*) was used to arrest embryos in Metaphase I for XFM [25]. JK560 (*fog-1(q253)I*) was used in TPEN challenge experiments [26]. GH378 (*pgp-2(kx48)I*) was used in in vivo labile zinc fluorescence experiments [27].

Growth media

All control animals were grown on Nematode Growth Media plates [28] seeded with an OP50 bacterial lawn. Worms were similarly plated on nematode growth media (NGM) infused with TPEN at a final concentration of 10 μM (Sigma Aldrich, St. Louis, MO) for XFM experiments.

Imaging buffers

Egg buffer

The egg buffer for meiotic progression experiments and TPEN challenge experiments was supplemented with 100 nM ZincBY-1. The components included 25 mM 4-(2-hydroxyethyl)-1-piperazineethanesulfonic acid (HEPES), pH 7.3, 118 mM NaCl, 48 mM KCl, 2 mM $CaCl_2$, and 2 mM $MgCl_2$ [29].

Meiosis media

The meiosis media for meiotic progression experiments was supplemented with 50 or 100 nM ZincBY-1. The components include 5 mg/mL Inulin in culture safe water, 25 mM HEPES, 60% Leibowitz L-15 media, and 20% Heat Inactivated Fetal Bovine Serum (Fisher) [30].

Zinc probes

Experiments that monitor dynamic changes in the localization of labile zinc in isolated embryos utilize ZincBY-1 ($\lambda_{ex} = 520$ nm, $\lambda_{em} = 543$ nm) [23]. All dilutions were made in M9 buffer.

X-ray fluorescence microscopy sample preparation

Whole gonad isolation

L4 stage N2 worms were synchronized at 20°C on NGM plates and were grown until they were day 1 adults, before dissecting the gonads with a 20-gauge needle into 0.1 M aqueous ammonium acetate buffer on a microscope slide. Worms were cultured under control conditions (NGM alone), or on plates infused with 10 μM TPEN.

Analysis of meiotic and mitotic stages

Animals were bisected near the vulva to obtain wild-type embryos (N2) in meiotic ($n = 7$), 1-cell ($n = 10$) and 2-cell stages ($n = 9$); selected cell stages were based on presence of polar bodies and visualization of pronuclei and nuclei. For the metaphase arrest experiment, L4 stage AV335 worms containing a temperature-sensitive mutation in Anaphase Promoting Complex component *emb-27* were cultured overnight at 20°C and then shifted to 25°C for 7 h to induce metaphase I arrest, before dissecting into 0.1 M ammonium acetate buffer and mounting them similarly to isolated gonads ($n = 15$).

X-ray fluorescence microscopy scanning parameters and analysis

Samples for XFM were mouth pipetted onto silicon nitride windows after dissecting in ammonium acetate buffer, followed by air drying. Note that air drying can sometimes distort the shape of the cells (which may explain the stretched appearance of some of the cells in Figure 1B). Isolated 1-cell and 2-cell stage embryos were raster scanned at a 50 ms dwell time at a 2 μm step size and isolated MI stage embryos were raster scanned at 100 ms dwell time at a 5 μm step size. Larger, isolated gonads were raster scanned at a 15 ms dwell time at a 5 μm step size and the fluorescence data were analyzed using the MAPS software [31]. A beam splitting Si (220) monochromator focused the X-ray beam using Fresnel zone plates at an energy of 10 keV and provided a focused beam size of 0.5 μm × 0.4 μm. All XFM experiments were performed at the 2-ID-E beamline at the Advanced Photon Source (Argonne National Laboratory in Argonne, IL).

Statistical analysis of XFM experiments

For meiotic progression experiments, the total content of a given element is reported in units of atoms/cell. Statistical significance was determined by first performing a two-way ANOVA analysis to test the interaction between each metal and stage using Prism GraphPad. A two-way analysis of variance (ANOVA) analysis showed a significant interaction ($P < 0.0001$) between the meiotic stage and metal content. Because this interaction was significant, we followed the ANOVA with a Student *t*-test comparing the given total metal content to each stage of meiotic progression; *P*-values below 0.05 were considered statistically significant. Significance is designated by letters assigned to meiotic stage. Letters that are the same are not statistically significant. For experiments measuring metal content in individual oocytes within dissected gonads, we performed a one-way ANOVA analysis to test the interaction between total metal content and each oocyte occupying the −4 through −1 positions. In all cases, $P > 0.05$, so the interaction between total metal content and oocyte position was not considered significant.

Confocal fluorescence microscopy

Isolated embryos for meiotic progression experiments

All meiotic progression experiments in isolated embryos were conducted on a Leica SP5 II Laser Scanning Confocal Microscope located at the Biological Imaging Facility at Northwestern University. Control embryos were dissected from day 1 adult hermaphrodites (EU1067) directly into 7 μL of either 50 or 100 nM ZincBY-1 as indicated [23] in a 35-mm glass bottom FluoroDish (World Precision Instruments). Time-lapse videos were acquired at room temperature using the 63× objective and captured with the HyD detector, the 488 laser to detect GFP and the 514 laser to detect ZincBY-1. Videos were captured at 60-s intervals with a 0.8 μm step size, in short segments of meiosis (~10–20 min, $n = 11$). Imaging using 50 nM ZincBY-1 ($n = 7$) eliminated probe chelation effects and allowed for complete imaging of meiosis. Embryos were collected across seven experiments. For each experiment, we dissected, screened, and scanned four to six embryos (total screened, $n = 28$–42). Screening and scanning involved eliminating embryos that were progressing outside of meiosis. For each dissection, we identified one embryo at a time that was progressing through meiosis. Embryos that were identified at Meiosis I were imaged continuously through the 2-cell stage. Others that were in later stages of meiosis were also imaged, and the data were pooled to acquire fluorescence intensity per stage across all embryos representing Metaphase I to 2-cell ($n = 7$).

Preparation of live worms

For in vivo experiments, we adapted the worm preparation protocol [32] by reconstituting 5-mM ZincBY-1 or Fluozin-3 AM (Invitrogen) stock solution in dimethylsulfoxide (Sigma) and diluting in M9 buffer (22 mM KH_2PO_4, 42 mM Na_2HPO_4, 86 mM NaCl) [29] to a final concentration of 50 mM. All live worm experiments used a serotonin-dye solution. We dissolved serotonin creatinine sulfate (Sigma) in M9 buffer to a final concentration of 50 μM while sonicating and mildly heating (50°C). Next, we picked young adult animals in 100 μL of 50 μM ZincBY-1 ($n = 11$) or Fluozin-3 ($n = 4$) solution and incubated in the dark at 20°C for 3–4 h. The 50 μM dye solution containing the soaking live worms was dispensed onto an NGM plate with OP50 and the worms were allowed to recover for up to 150 min.

Imaging and analysis of live worms

We adapted the live worm imaging protocol [33] and immobilized dye-soaked worms on a 3% agarose pad using a few droplets of a mixture of equal parts 0.1 μm polystyrene beads (Polysciences) and 50 μM serotonin creatinine sulfate. Next, we imaged animals on a Leica

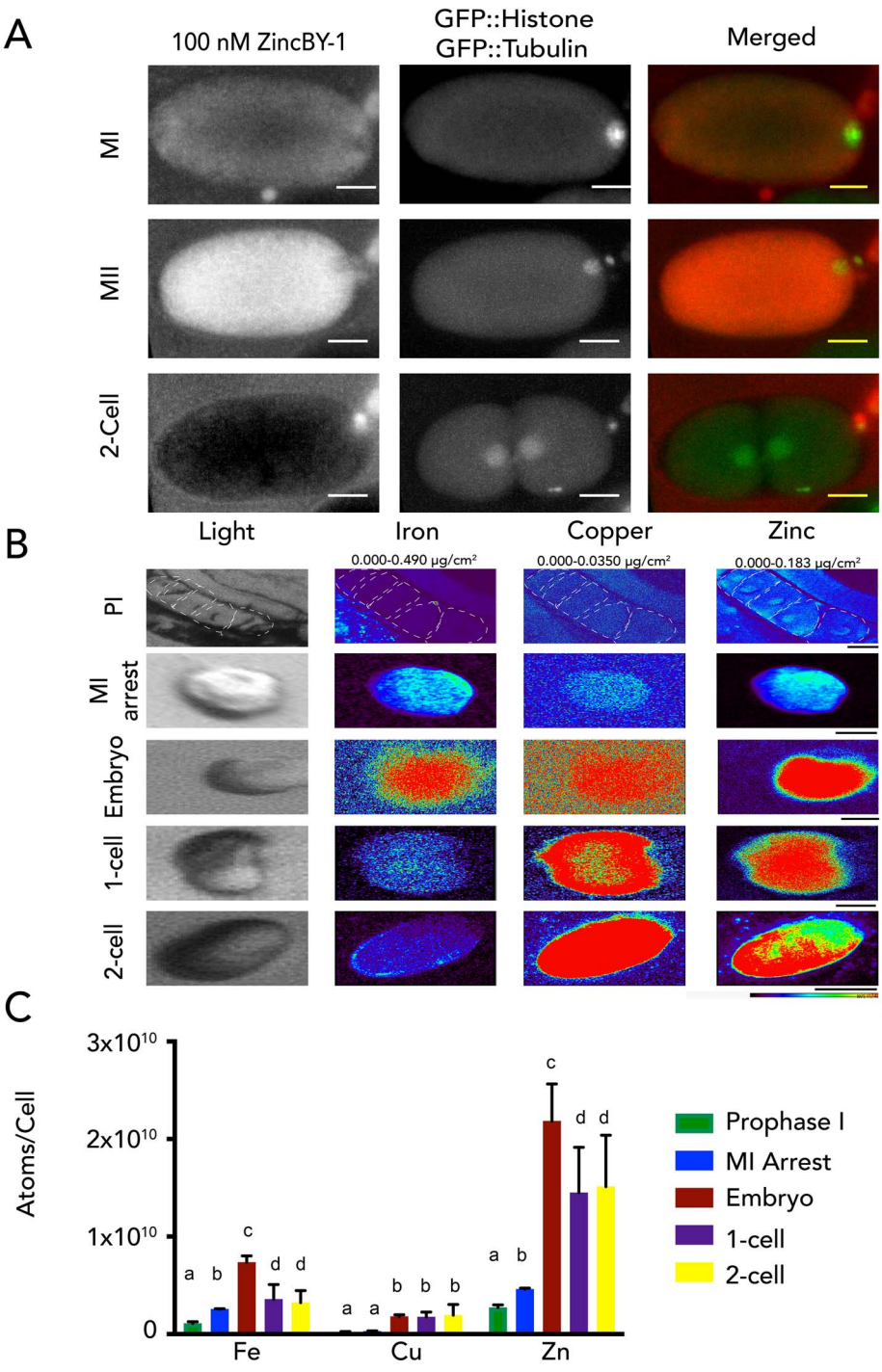

Figure 1. Transient changes in both labile and total zinc in *Caenorhabditis elegans* oocytes and embryos across meiotic and early mitotic stages. (A) The distribution of labile zinc using ZincBY-1 fluorescence as a reporter (left column, red in the merge). Developmental stages were assigned using a worm strain expressing GFP::tubulin and GFP::H2B histone (middle column, green in the merge). Labile zinc is apparent throughout the cytoplasm in MI ($n = 2$) and increased significantly as cells enter MII ($n = 5$). Finally, labile zinc in the 2-cell embryo ($n = 5$) is not apparent in the cytoplasm but is apparent in the eggshell in seven experiments. Scale bar = 10 μm. (B, C) Total zinc, copper, and iron content at the single cell level was established using XFM across four experiments and is shown in units of atoms/cell. Example images are shown in B and quantification is shown in C; the number of cells analyzed for each stage was greater than 7. Most of the stages were analyzed in wild-type (N2) worms (Prophase I, $n = 15$; Embryo, $n = 7$; 1-cell, $n = 10$; 2-cell, $n = 10$), except for the Metaphase I-arrest stage ($n = 15$), which was assessed in worms with a temperature-sensitive mutation in the anaphase-promoting complex component *emb-27*. In wild-type, the "embryo" stage refers to fertilized embryos undergoing the meiotic divisions, whereas the "1-Cell" and "2-Cell" stages are in mitosis. Total Zn content increased by more than threefold between Metaphase I and the embryo stage. Fe and Zn generally display a similar flux pattern across the meiotic and mitotic stages. Scale bar = 10 μm (1-cell) and 20 μm (PI, MI, and 2-cell). The color legend indicates the spectrum of intensity of total zinc with blue being low intensity, and low levels of total zinc, and red being high intensity and high levels of total zinc. (C) The letters above the bars represent statistical significance between developmental stages for the given element where $P < 0.05$. Letters that are the same are statistically insignificant ($P > 0.05$). Statistical analysis was conducted by performing a one-way ANOVA followed by a Student *t*-test.

DMI6000 Spinning Disk Inverted Confocal Microscope with a Yokogawa CSU-X1 spinning disk module with a Microlens-enhanced Nipkow disk and a Photometrics Evolve Delta512 camera. Animals were captured using a 20× air objective and 488 and 561 nm solid state lasers and images were processed and analyzed using Fiji software [34, 35].

Tests for zinc-specific fluorescence in embryos and oocytes

To test whether the observed fluorescence signal arose from zinc and not from auto-fluorescence, we imaged isolated gonads on the same Leica SP5 II laser Scanning Confocal Microscope as the isolated embryos, and also carried out controls where excess TPEN was added. Since TPEN binds zinc five to six orders of magnitude more tightly than ZincBY-1, addition of excess TPEN removed zinc from the probe and allowed measurement of background fluorescence. We dissected oocytes and embryos from wild-type (N2) and *fog-1(q251)* animals into Egg buffer alone, 10 μL of buffer containing 75 nM ZincBY-1 ($n = 5$), 10 μL of 75 nM ZincBY-1 + 50 μM TPEN ($n = 5$), 10 μL of 75 nM ZincBY-1 + 10 μM Zn pyrithione ($n = 5$), and 50 μM TPEN alone ($n = 5$). All samples were incubated for 15 min and were then covered with a coverslip that was slightly elevated with high vacuum grease beads (Dow Corning). To ensure that changes in ZincBY-1 fluorescence intensity were due to biological changes within the embryos, we conducted photobleaching controls using an 8 μL drop of 50 nM ZincBY-1 under mineral oil for 15 min with the 514 laser and scanned a depth of 30 μm at a 0.8 μm step size. In addition, 8 μL of ZincBY-1 only was imaged under mineral oil (Sigma) using the same imaging settings as was used for isolated embryos. ZincBY-1 only samples were imaged at 0.8 μm at a depth of 42 μm.

Fluorescence microscopy data analysis

Quantifying fluorescence of oocytes in live worms

In ImageJ, three squares of equal area were drawn within each distinguishable oocyte and three squares of the same size were drawn in the background (outside the worm). Next, the mean fluorescence intensity of each box was measured from a single slice, then the values for these boxes were averaged to generate an average fluorescence intensity value of the oocyte or background. To get the true fluorescence intensity, the average intensity of the background was subtracted from each oocyte average. To account for variation, we normalized the fluorescence intensities by setting the background corrected "-1" oocyte value to 100%.

Cytoplasmic volume estimation in isolated embryos

The EU1067 strain (*unc-119(ed3) ruIs32[unc-119(+) pie-1^{promoter}::GFP::H2B]III; ruIs57[unc-119(+)pie-1^{promoter}::GFP::tubulin]*) was advantageous because we could define the cytoplasm using GFP::tubulin fluorescence. The Volumest plugin [36] in ImageJ was used to estimate the cytoplasmic volume (reported as μm^3).

Fluorescence intensity measurements in isolated embryos

Fluorescence intensity was determined for each channel by using the sum slice max projection in Image J. From this projection, we performed background subtraction by rolling ball radius based on the number of pixels/embryo. We measured the fluorescence intensity by selecting an region of interest (ROI) of the cytoplasm as defined by GFP::tubulin (EU1067) and used that same ROI to define the cytoplasm by ZincBY-1 in the sum slice analysis. After obtaining the fluorescence intensity measurements and the volume measurements for each stage, we plotted ZincBY-1 intensity as fluorescence intensity/volume.

Quantifying defects in the embryos

Pronuclei were identified using the GFP::tubulin and GFP::histone markers. We assessed (1) the formation of one pronucleus on each side of the embryo (2 total), (2) if they joined together in the normal time frame following the completion of meiosis, and (3) if a normal mitotic spindle formed. These features were assessed using time-lapse microscopy. We used these same criteria when assessing embryos exposed to TPEN. If any of these criteria were unmet, it was considered abnormal.

Results

Transient changes in labile zinc occur during late oocyte maturation in *C. elegans*

To determine whether fluctuations in labile zinc occur during germ cell maturation in *C. elegans*, we used live cell fluorescence microscopy to examine oocytes treated with the zinc responsive fluorescent probe, ZincBY-1 [23]. This zinc probe is cell-permeable and has been successfully used at nanomolar concentrations in mouse oocytes. Moreover, unlike molecular probes containing AM-ester functionalities, it does not require an enzyme cleavage mechanism to function [37]. Worm strains expressing GFP::tubulin and GFP::histone were used to allow real-time correlation with spindle dynamics [25], thus facilitating the identification of specific cell cycle stages. In *C. elegans*, Prophase I oocytes are fertilized, and this triggers the assembly of the oocyte spindle and progression through the meiotic divisions. Following the extrusion of the second polar body, the female and male pronuclei fuse and then begin the mitotic divisions of the embryo. Initially we surveyed comparable stages to those previously documented in mammals: Metaphase I, Metaphase II, and the 2-cell mitotic embryo. ZincBY-1 fluorescence was abundant in the cytoplasm of Metaphase I and Metaphase II cells but was significantly diminished in the 2-cell mitotic stage (Figure 1A).

To establish whether ZincBY-1 fluorescence in *C. elegans* embryos was zinc specific, we used a series of reagents that perturb zinc availability and employed a worm strain, *fog-1(q253)* [26, 38], which does not produce sperm; at the restrictive temperature (25°C), oocytes from these animals remain unfertilized, do not advance through the cell cycle, and do not undergo changes in eggshell permeability, thereby ensuring that zinc probe and zinc-perturbing reagents will permeate the oocyte membrane without risk of blocking by the eggshell. We found that addition of the cell-permeable zinc chelator TPEN, which binds zinc much more avidly than ZincBY-1, eliminated fluorescence in ZincBY-1-treated *fog-1(q253)* oocytes (Supplementary Figure S1A, ii, iii). As expected, addition of 10 μM zinc pyrithione, a zinc ionophore, increased fluorescence (Supplementary Figure S1A, iv). Furthermore, fluorescence was not observed in *fog-1(q253)* oocytes that were not exposed to ZincBY-1, both with and without TPEN addition (Supplementary Figure S1A, i, v). A similar profile was seen in

isolated gonads. Gonads not exposed to ZincBY-1 showed no autofluorescence (Supplementary Figure S1B, i, vi). Gonads treated with ZincBY-1 displayed fluorescence (Supplementary Figure S1B, ii, vii), and this fluorescence was eliminated upon exposure to 10 μM TPEN (Supplementary Figure S1B, iii, viii). Addition of 10 μM zinc pyrithione increased fluorescence (Supplementary Figure S1B, iv, ix). Exposure to 10 μM TPEN alone showed no fluorescence (Supplementary Figure S1B, v, x). Finally, exposure of wild-type embryos to 10 μM TPEN reduced ZincBY-1 fluorescence (Figure 2A and B), similar to the *fog-1(q253)* results. We further performed a control experiment with ZincBY-1 alone in meiosis media to determine if the zinc dye was susceptible to photobleaching under our imaging conditions. ZincBY-1 exposure to the confocal laser did not show a reduction in fluorescence signal over time (Movie 1, Supplementary Figure S2). These results and controls support the conclusion that labile zinc levels in the cytosol of germ cells increase during meiosis and decrease as the cells progress to early mitotic stages (Figure 1A). This flux in labile zinc concentration may arise from zinc import or from the release of zinc from binding sites that are not accessible to the probe. One way to address this question is to measure the total zinc content at the single cell level.

Total zinc content increases substantially after metaphase I

To determine if changes in the total cellular content of zinc occur in parallel with labile zinc in a stage-specific manner, we examined isolated *C. elegans* oocytes and embryos using synchrotron-based XFM. Quantitative analysis of changes in zinc content was obtained by deconvoluting X-ray emission spectra into element-specific photon counts within a given *x*-*y* region into numbers of atoms of that element, as described previously [15]. All X-ray photons emitted from the sample are integrated across the *z*-axis, so the number of atoms in a given *x*-*y* ROI corresponds to the sum of atoms in *x*, *y*, *z*. We evaluated multiple stages in wild-type animals including Prophase I oocytes, fertilized embryos undergoing the meiotic divisions (we were not able to stage them more precisely since spindle dynamics were not visible using this technique), and mitotic 1-cell and 2-cell stage embryos; we also used a temperature sensitive mutant to analyze oocytes arrested at Metaphase I [25] (Figure 1B). For this analysis, we defined the ROI by cellular boundaries using the phase contrast images, and the number of atoms within the ROI is represented as atoms/cell (Figure 1C).

First, we tested whether oocytes within the gonad undergo changes in total and labile zinc content prior to fertilization. The −1 oocyte is located adjacent to the spermatheca and is the only one that can be fertilized. Oocytes further away from the spermatheca are numbered in descending order [39] (Supplementary Figure S3A). Experiments utilizing ZincBY-1 revealed a modest increase in labile zinc in oocytes from the −4 to the −1 position of the germ line (Supplementary Figure S1C and D). However, XFM analysis (Supplementary Figure S3B and C) revealed that the total zinc content did not significantly increase ($P > 0.05$) as the oocyte progressed from the −4 to the −1 position (Table 2). Although the total zinc concentration in these oocytes was constant, we find the highest zinc localized in the nucleus.

In contrast, comparison of wild-type Prophase I oocytes with fertilized meiotically dividing embryos revealed that total zinc content increased by nearly an order of magnitude between these two stages ($2.7 \pm 0.27 \times 10^9$ in Prophase compared with $2.2 \pm 0.38 \times 10^{10}$ in embryos) (Figure 1C). To more precisely define when in the cell cycle this increase occurs, we examined embryos from a *C. elegans* strain with a temperature-sensitive mutation in the anaphase-promoting complex, which leads to a Metaphase I arrest at the restrictive temperature. The average number of zinc atoms/cell at Metaphase I ($4.6 \pm 0.11 \times 10^9$) was only slightly higher than at Prophase I, indicating that most of the zinc accumulation occurs after Metaphase I (Figure 1C). Total zinc levels then decreased slightly after progression from meiosis to the 1-cell ($1.5 \pm 0.47 \times 10^{10}$) or 2-cell ($1.5 \pm 0.53 \times 10^{10}$) mitotically dividing embryo (Table 1). Regardless of stage, zinc was the most abundant transition metal in these oocytes and embryos. Total iron and copper content also increased across this developmental window (Figure 1B and C); iron increasing by 560% and copper by 640% between Prophase I and the embryo compared with zinc, which increased by 700%. In mammalian oocytes, the absolute increase in zinc across these two stages is also much greater than is seen for iron and copper [12]. This pattern of iron, copper, and zinc changes in *C. elegans* help frame our earlier observation that lowering of zinc, but not iron or copper, via metal-selective chelation disrupts these stages of meiosis [40]. Further experiments will be necessary to determine what role, if any, iron and copper might play in meiotic progression in *C. elegans*. However, the large changes in total zinc content are significant and follow a similar pattern to changes in labile zinc, where we observed a rapid increase as cells entered the MII stage and a decrease in metal content in the mitotic cells, motivating us further examine zinc during early embryonic development.

Induced zinc insufficiency leads to developmental defects

Previously, we and others reported that zinc insufficient zygotes can experience impairments in the extrusion of the second polar body [40, 41]. To test whether zinc restriction also alters the subsequent mitotic divisions, isolated individual embryos were dissected directly into buffer containing 100 nM ZincBY-1 and 10 μM TPEN prior to eggshell deposition, and then subjected to time-lapse imaging as the embryos progressed through the cell cycle. ZincBY-1 fluorescence decreased upon TPEN treatment prior to eggshell deposition in Anaphase I and stayed low throughout the cell cycle (Figure 2A and B), confirming that this treatment restricted intracellular zinc availability across this time frame. This is in contrast to control embryos that were not exposed to TPEN, which showed a strong ZincBY-1 fluorescence increase from Anaphase I to a Metaphase II peak, followed by a diminished fluorescence signal at pronuclear formation (Figure 2A and B). As before, we observed abnormalities in all embryos exposed to TPEN ($n = 14$) (Figure 2C–G). Of the total number of embryos analyzed, 21% (3/14) contained ≥3 pronuclei, 50% (7/14) displayed a retraction or retention of the second polar body, 57% (8/14) had abnormal pronuclear migration, and 36% (5/14) had mitotic spindle positioning defects (Figure 2F; note that these percentages add up to >100% since every embryo had multiple defects).

Given these phenotypes, we next assessed whether TPEN-treated embryos were able to progress to the 2-cell stage; this

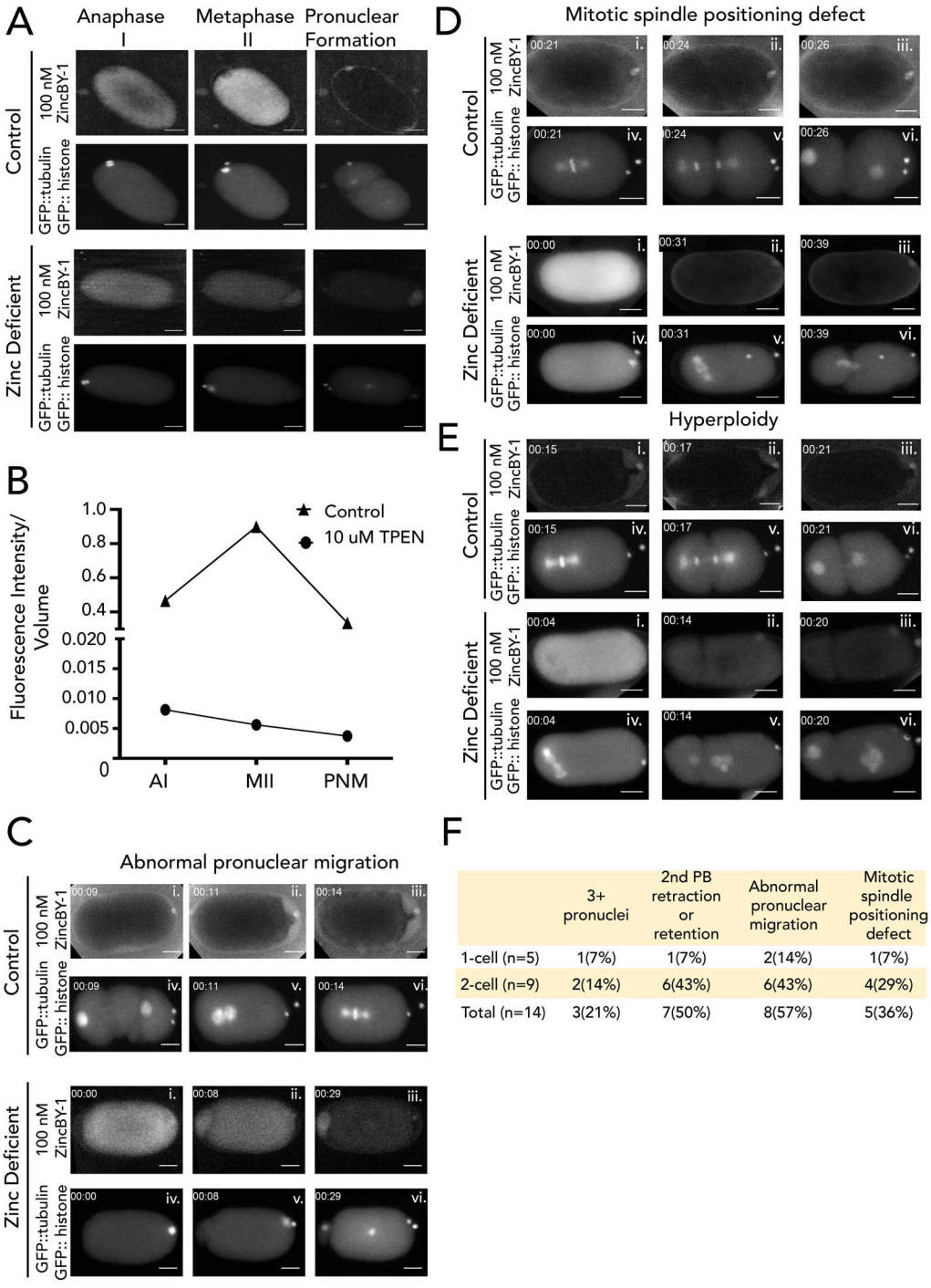

Figure 2. Blocking zinc influx with TPEN induces a series of meiotic defects. Fluorescence images are of embryos expressing GFP::histone and GFP::tubulin (bottom row of images) and treated with 100 nM ZincBY-1 (top row of images). (A, B) Control embryos that cycle through the meiotic divisions show an increased uptake of ZincBY-1 fluorescence from Anaphase I to Metaphase II. Compared with controls, embryos treated with 10 μM TPEN at Anaphase I prior to eggshell formation show decreased ZincBY-1 fluorescence intensity that continuously drops through pronuclear formation. (C–E) Embryos were dissected into 10 μM TPEN, mounted, and filmed. T = 0 represents the beginning of filming. ZincBY-1 and GFP pairs are from the same movie. (C) A pronucleus is trapped in the posterior end of the embryo and is contained within a small portion of the cytoplasm as ZincBY-1 fluorescence decreases (i–iii) and the cell cycle progresses (iv–vi). (D) iv–vi shows a mitotic spindle in the posterior end of the embryo oriented perpendicularly, demonstrating defects in spindle positioning. ZincBY-1 fluorescence also decreases (i–iii). (E) iv–vi shows a misoriented mitotic spindle and extra nuclei as a result of mitotic defects, whereas ZincBY-1 fluorescence decreases during pronuclear migration (i–iii). (F) All embryos were collected in five experiments ($n = 14$) and were exposed to 10 μM TPEN contained meiotic defects: 21% ($n = 3/14$) contained 3 or more pronuclei, 50% ($n = 7/14$) had retraction or retention of the second polar body, 36% ($n = 5/14$) had mitotic spindle positioning defects, and 57% ($n = 8/14$) had abnormal pronuclear migration leading to hyperploidy. Despite the defects, the embryos could still progress to the 1-cell ($n = 5$) or 2-cell stage ($n = 9$). All scale bars = 10 μm.

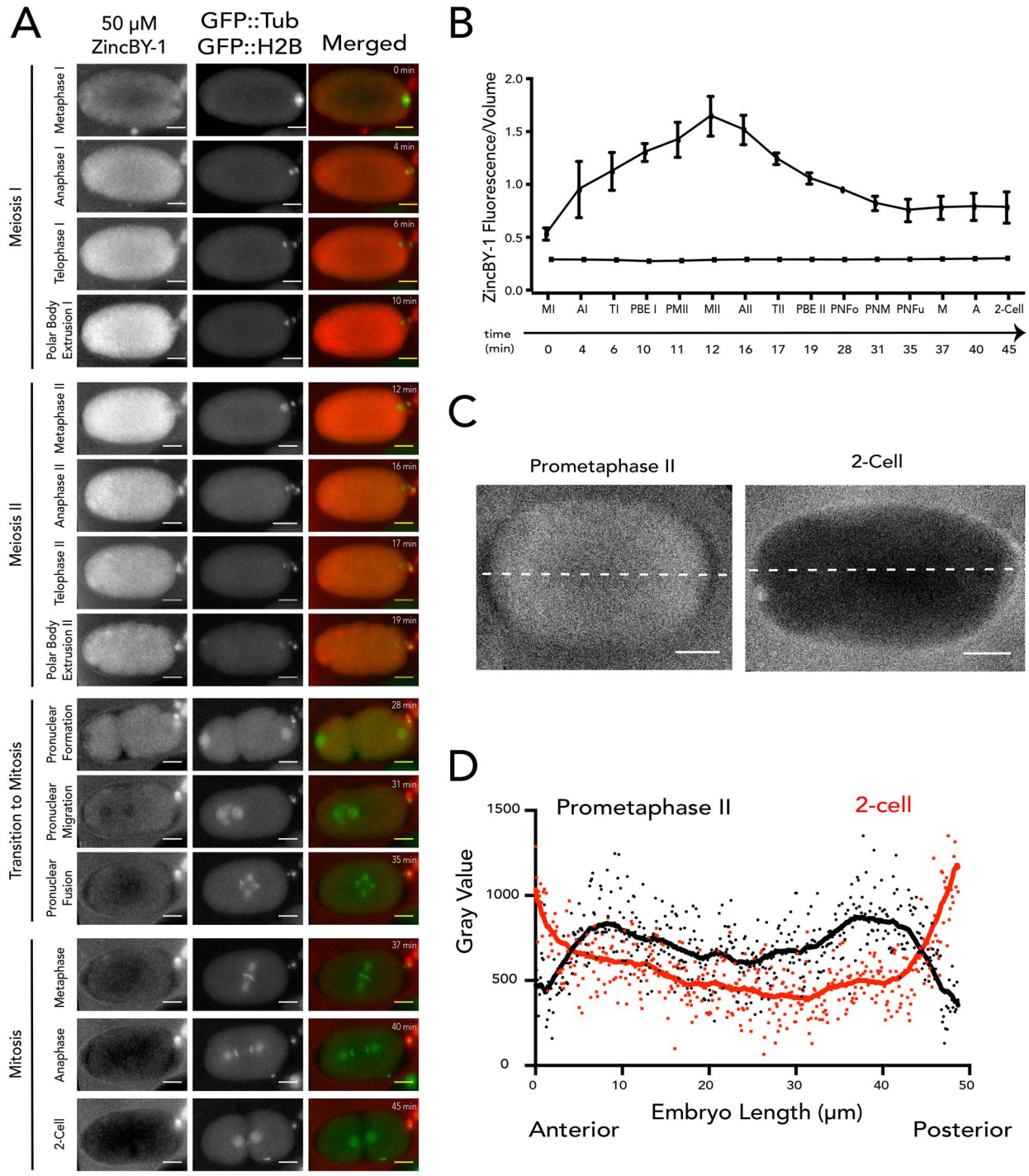

Figure 3. Live-cell microscopy reveals labile zinc fluxes during meiotic progression. (A) Cells treated with ZincBY-1 (left column, red in merge) exhibit a significant increase in fluorescence as they progress from Meiosis I to Meiosis II; total fluorescence then begins to decrease at Anaphase II and continues to drop through pronuclear fusion. Fluorescence levels then remain low through the 2-cell stage. (B) Plot of the integrated fluorescence intensity normalized to cell volume is consistent with a threefold fluctuation in labile zinc that occurs in a stage-specific manner across meiotic maturation ($n = 7$ embryos isolated from 7 animals). Error bars represent standard error of mean. (C) Fluorescence images comparing ZincBY-1 fluorescence in Prometaphase II to the 2-cell stage. Cytoplasmic fluorescence is lower at the 2-cell stage, but there is increased fluorescence at the periphery of the embryo. (D) A fluorescence comparison by gray value of Prometaphase II compared with the 2-cell stage, showing that labile zinc is fairly uniform across the cytoplasm in Prometaphase II, but after completion of meiosis is enriched in the eggshell region ($n = 5$, 2 experiments). All scale bars = 10 μm.

is an important issue because previous mouse experiments demonstrated that TPEN exposure arrested the cell cycle [12]. In contrast to mouse, we found that 62% of all *C. elegans* embryos exposed to TPEN (9/14) were able to progress to the 2-cell stage despite experiencing several meiotic defects, whereas five arrested at the 1-cell stage (Figure 2F). We conclude that the large increase in zinc content in the late meiotic stage is necessary for normal embryo development but

Table 1. Quantification of elements during meiotic progression in the *C. elegans* embryo

	Prophase I (N2)			MI Arrest (AV335)			Embryo (N2)			1-Cell (N2)			2-Cell (N2)		
	Mean	SEM	N	Mean	SEM	N	Mean	SEM	N	Mean	SEM	N	Mean	SEM	N
P	8.87×10^{11}	6.76×10^{10}	15	7.79×10^{11}	2.19×10^{10}	15	5.09×10^{12}	7.29×10^{11}	7	2.40×10^{12}	8.88×10^{11}	10	2.72×10^{12}	9.97×10^{11}	9
Fe	1.10×10^{9}	1.72×10^{8}	15	2.56×10^{9}	5.42×10^{7}	15	7.35×10^{9}	6.64×10^{8}	7	3.57×10^{9}	1.51×10^{9}	10	3.23×10^{9}	1.24×10^{9}	9
Cu	2.43×10^{8}	2.76×10^{7}	15	3.19×10^{8}	1.36×10^{7}	15	1.79×10^{9}	1.96×10^{8}	7	1.75×10^{9}	5.05×10^{8}	10	1.95×10^{9}	1.08×10^{9}	9
Zn	2.72×10^{9}	2.68×10^{8}	15	4.61×10^{9}	1.13×10^{8}	15	2.19×10^{10}	3.81×10^{9}	7	1.45×10^{10}	4.66×10^{9}	10	1.51×10^{10}	5.29×10^{9}	9

Mean number of atoms/cell of phosphorus (P), iron (Fe), copper (Cu), and zinc (Zn) in the Prophase I ($n = 15$), Metaphase I arrest ($n = 15$), Embryo ($n = 7$), 1-cell ($n = 10$), and 2-cell ($n = 9$) stages. Note that phosphorus was included in the analysis because maps of this element are routinely used to delineate cell boundaries.

preventing this increase with TPEN does not completely block cell cycle progression and some embryos are able to advance to the 2-cell stage with defects.

A second significant zinc flux begins during Anaphase II

To better understand the spatial and temporal dynamics of the zinc increase up to MII and the subsequent decrease as the fertilized oocyte begins entry into mitosis, we followed single embryos in live cell imaging across the egg-to-embryo transition. Corroborating the drop in total zinc between Prophase I and the one-cell embryo, we observed a decrease in cytoplasmic ZincBY-1 fluorescence beginning in Metaphase II (Figure 3A and B, Movie 2). Notably, this decrease correlated with a steady increase in fluorescence near the periphery of the embryo (Figure 3C). This increased fluorescence was in the region of the eggshell, a multilayer structure that functions as a polyspermy block, protects the embryo from the environment, and maintains embryo osmolarity [42–45]. By the 2-cell mitotic stage, ZincBY-1 fluorescence was detected in the space between the cytoplasm and an outer eggshell layer (Movie 3). Line scans across embryos at Prometaphase II showed elevated ZincBY-1 fluorescence in the inner 30 μm of the embryo, corresponding to the cytoplasm, compared with the outer 10 μm of each side of the cytoplasm, corresponding to the anterior and posterior poles. In contrast, the 2-cell stage embryo showed the inverse concentration of labile zinc, which was lower in the cytoplasm compared with the eggshell region (Figure 3C and D, Movie 3).

The time-lapse experiments (Figure 3A and B) were conducted with long-term exposure to ZincBY-1 throughout meiotic progression. To determine whether continuous exposure of the embryo to the probe might alter labile zinc exocytosis and therefore lead to accumulation in the eggshell, we limited ZincBY-1 exposure time to 1 min while the early zygote was permeable and followed with a buffer rinse to remove excess probe. We found no difference between short term and continuous exposure to the probe: fluorescence accumulated in the same manner across the eggshell region and cell division progressed normally (Movie 4), indicating that the probe did not alter labile zinc distribution in the eggshell region over time. We conclude that significant, large-scale fluxes in labile zinc occur between fertilization and mitotic entry. Labile intracellular zinc levels begin rising in prophase oocytes, and then increase sharply after fertilization and peak around Metaphase II. These levels then decrease until the pronuclear formation stage; during this decrease in the cytoplasm, the eggshell region acquires labile zinc that remains there in the 2-cell stage mitotic embryo.

Discussion

Zinc fluxes are essential to oocyte maturation and egg viability in *C. elegans*

These results in *C. elegans* provide the first direct spatial temporal correlation of cell cycle and zinc flux events during the egg-to-embryo transition. Our findings also expand the evolutionary scope of dynamic zinc fluxes and strongly support the idea that cyclic changes in zinc are a major factor in developmental pathways controlling both the oocyte-to-egg and egg-to-embryo transitions across

Table 2. Quantification of elements in *C. elegans* oocytes.

	−1			−2			−3			−4		
	Mean	SEM	N	Mean	SEM	N	Mean	SEM	N	Mean	SEM	N
P	8.07×10^{11}	6.76×10^{10}	5	8.30×10^{11}	5.43×10^{10}	5	7.67×10^{11}	3.13×10^{10}	5	6.50×10^{11}	6.31×10^{10}	5
Fe	1.97×10^{9}	3.19×10^{8}	5	1.60×10^{9}	2.18×10^{8}	5	1.46×10^{9}	1.36×10^{8}	5	1.36×10^{9}	1.75×10^{8}	5
Cu	2.59×10^{8}	3.85×10^{7}	5	2.28×10^{8}	2.37×10^{7}	5	2.00×10^{8}	1.38×10^{7}	5	1.94×10^{8}	2.74×10^{7}	5
Zn	3.83×10^{9}	4.44×10^{8}	5	3.67×10^{9}	3.86×10^{8}	5	3.54×10^{9}	1.28×10^{8}	5	53.40×10^{9}	3.63×10^{8}	5

Mean number of atoms/cell of phosphorous (P), iron (Fe), copper (Cu), and zinc (Zn) in the −1 oocyte ($n = 5$), −2 oocyte ($n = 5$), −3 oocyte ($n = 5$), and − 4 oocyte ($n = 5$). Note that phosphorus was included in the analysis because maps of this element are routinely used to delineate cell boundaries.

metazoans (Figure 4A). This conclusion is supported by earlier studies that showed that zinc limitation reduces *C. elegans* brood size and causes defects in oogenesis [40], including reduced oocyte number, an extended number of pachytene nuclei in the gonad, and improper oocyte stacking [46]. The importance of these cyclic changes in zinc concentration is born out in zinc limitation experiments; acute zinc limitation in isolated embryos disrupts polar body extrusion at the end of Meiosis II and leads to defects in spindle positioning, and hyperploidy [40] (Figure 4B).

Total and labile zinc change in parallel after fertilization

Although the maturing *C. elegans* oocyte shows a significant increase in the amount of labile zinc from the −4 to the −1 position of the germ line, the total zinc content does not change significantly from oocyte to oocyte. This may be attributed to labile zinc becoming liberated from tight binding sites that are not accessible to the zinc probe in oocytes closer to the loop region of the gonad. In this scenario, there would be no change in total zinc in the oocytes, but rather a change of zinc accessibility to probes. Alternatively, the influx of labile zinc may constitute a very small change in total zinc levels this would mean that labile zinc fluxes occur but would account for a very small change of the total zinc that would be difficult to detect in our XFM analysis. By contrast, the developing *C. elegans* embryo exhibits substantial and highly coordinated increases in total and labile zinc distribution as it progresses from Meiosis I to Meiosis II and then drops as the zygote transitions to mitosis (Figure 4A). This nicely parallels the fluctuations of total zinc in the mouse meiotic cell cycle; after Meiosis II the *C. elegans* embryo has lost 31% of total zinc compared with the mouse egg where 20% of the total ensemble of zinc ions are lost via cortical vesicle exocytosis [12]. It is quite interesting that this general flux pattern persisted throughout evolution, despite differences in meiotic regulation between *C. elegans* and mammals. A notable difference is the timing of the zinc fluxes relative to fertilization. In *C. elegans*, oocytes are ovulated and then fertilized prior to the initiation of the meiotic divisions [47]. Thus, in this organism, zinc influx largely occurs after fertilization; once influx begins, dynamic changes occur continuously with efflux beginning at Metaphase II and ending at the start of Mitosis (Figure 3A, B and Figure 4A). In contrast, mouse oocytes arrest at Metaphase II, and then fertilization triggers the release from this arrest. In mouse, zinc efflux occurs as cortical granule release upon this fertilization-induced resumption of the cell cycle. These differences in zinc efflux relative to the timing of fertilization suggest that fertilization is not a universal trigger for zinc efflux, and instead demonstrates that alternative mechanisms must control zinc influx and efflux. Whether zinc influx is linked to mechanisms that promote meiotic maturation such as major sperm protein signaling is an open question.

Labile zinc accumulates in the eggshell during the transition from meiosis to mitosis

When the mouse egg transitions out of Meiosis II, rapid loss of zinc is readily detected as "zinc sparks" using extracellular probes. In contrast, as the *C. elegans* egg exits Meiosis II, the rapid loss is detected as an accumulation of labile zinc in the eggshell region (Figure 4C). The *C. elegans* eggshell has many functions, including osmolarity maintenance, polyspermy block, and protection from the environment [45, 48]. Here we show that labile zinc is distributed within the entire eggshell region (i.e., the space between the plasma membrane and the outermost eggshell layer). The comparable mammalian structure is the ZP. The ZP is a glycoprotein matrix that surrounds maturing mammalian oocytes. It undergoes structural changes during maturation and again after fertilization. After the sperm fuses with the egg, the ZP "hardens", and this hardening prevents polyspermy [16]. It was recently shown that post egg activation and endogenous zinc release or following addition of zinc to isolated ZPs, the fibril structure thickens in a manner identical to egg hardening [16, 23]. Recent studies suggests that the zinc release also contributes to the prevention of polyspermy in nonmammalian model systems, including the African clawed frog [18, 49] as well as salamander, zebrafish, and Cnidarians [49]. Whether and how extracellular zinc modifies the eggshell in *C. elegans* remains to be investigated more deeply.

Taken together, our results show that although most of the zinc in the cell is tightly bound to proteins and unavailable to fluorescent probes, transient fluctuations in labile zinc are highly correlated with two stages in meiotic maturation in *C. elegans*. Upon fertilization, a significant influx of zinc raises the total zinc concentration by over sevenfold and an increase in labile zinc is also observed, peaking at Metaphase II. Subsequent efflux events then reduce total zinc concentration by 31%, whereas the labile zinc concentration drops dramatically in the cytoplasm and increased in the eggshell region. This quantitative analysis of zinc fluxes during meiotic progression, both within the context of a single unfertilized oocyte and the developing embryo, establishes that zinc fluxes are characteristic of meiotic divisions and not mitotic ones. Further work in model organisms and in mammalian species will further explicate the important roles of zinc as a signal in meiotic cell cycle biology.

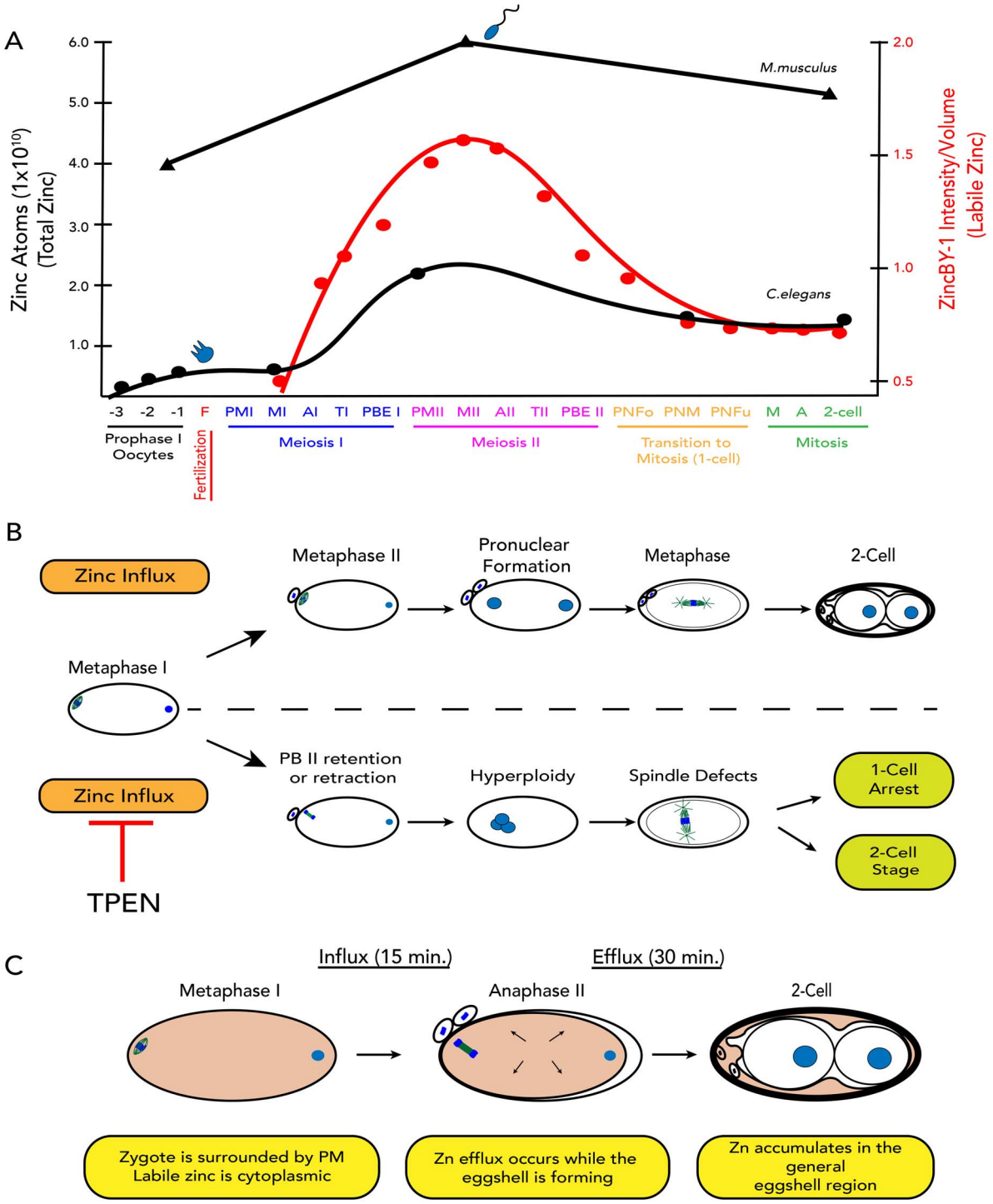

Figure 4. (A) Zinc fluxes in invertebrates have significant parallels to those seen in mammals. Both *C. elegans* and mouse oocytes accrue large quantities of total zinc during early stages of meiotic progression and achieve the maximum concentration at Metaphase II; total zinc then drops as the final phases of meiosis come to completion in both species. The timing of fertilization in both species is denoted by the presence of a blue sperm; in worm, fertilization occurs at the end of Prophase I, whereas in mouse, fertilization occurs at Metaphase II. Pronounced fluxes in labile zinc begin upon fertilization, which is restricted to different stages in the meiotic cycle, i.e., Prophase I in worm and Metaphase II arrest in mouse. (B) TPEN-induced zinc insufficiency in isolated, developing embryos experience polar body retention or retraction during Meiosis II, resulting in hyperploidy, spindle defects, and cell cycle arrest. (C) Labile zinc (pink) is acquired during the early stages of Meiosis I, when the embryo is permeable. Influx continuously occurs until Anaphase II, and then zinc is expelled from the cytoplasm over 30 min. Finally, labile zinc accumulates in the general eggshell region.

Author Contributions

A.D.M., S.M.W., T.K.W., and T.V.O. designed the research. A.D.M. and A.S. performed the experiments. O.A. and S.V. helped design and implement X.F.M. experiments, process and analyze the data. A.D.M., S.M.W., T.K.W., and T.V.O. wrote the manuscript.

Data availability

The data underlying this article will be shared on reasonable request to the corresponding author.

Supplementary material

Supplementary material is available at *BIOLRE* online.

Acknowledgements

Microscopy was performed at the Biological Imaging Facility at Northwestern University supported by the Chemistry of Life Processes Institute, the NU Office for Research, and the Department of Molecular Biosciences. Confocal microscopy was performed on a Leica TCS SP5 laser scanning confocal microscope system and the Leica Spining Disk Confocal Microscope; both were purchased with funds from the NU Office for Research. X-ray fluorescence microscopy was performed at the Advanced Photon Source (APS) at Argonne National Laboratory. We thank Dr J. Hornick for assistance with imaging, the Morimoto lab for the *fog-1 (q253)* strain, V. Pirsoul for figure preparation, and Ariella Coler-Reilly for designing the graphical abstract.

Conflict of interest

The authors declare no competing financial interests.

References

1. Hoch JA, Varughese KI. Keeping signals straight in phosphorelay signal transduction. *J Bacteriol* 2001; **183**:4941–4949.
2. Putney JW Jr. Ca2+ signaling. In: Siegel G, Agranoff BW, Alvbers RW (eds.), *Basic Neurochemistry: Molecular, Cellular and Medical Aspects*, 6th ed. Philadelphia: Lippincott-Raven; 1999: 379–390.
3. Andreini C, Banci L, Bertini I, Rosato A. Counting the zinc-proteins encoded in the human genome. *J Proteome Res* 2006; **5**:196–201.
4. Maret W. Metals on the move: zinc ions in cellular regulation and in the coordination dynamics of zinc proteins. *Biometals* 2011; **24**: 411–418.
5. Vallee BL, Falchuk KH. The biochemical basis of zinc physiology. *Physiol Rev* 1993; **73**:79–118.
6. Gilston BA, Wang S, Marcus MD, Canalizo-Hernandez MA, Swindell EP, Xue Y, Mondragon A, O'Halloran TV. Structural and mechanistic basis of zinc regulation across the *E. coli* Zur regulon. *PLoS Biol* 2014; **12**:e1001987.
7. Jackson KA, Valentine RA, Coneyworth LJ, Mathers JC, Ford D. Mechanisms of mammalian zinc-regulated gene expression. *Biochem Soc Trans* 2008; **36**:1262–1266.
8. Patzer SI, Hantke K. The zinc-responsive regulator Zur and its control of the znu gene cluster encoding the ZnuABC zinc uptake system in *Escherichia coli*. *J Biol Chem* 2000; **275**:24321–24332.
9. Bird AJ, Blankman E, Stillman DJ, Eide DJ, Winge DR. The Zap1 transcriptional activator also acts as a repressor by binding downstream of the TATA box in ZRT2. *EMBO J* 2004; **23**:1123–1132.
10. Coleman JE. Zinc proteins: enzymes, storage proteins, transcription factors, and replication proteins. *Annu Rev Biochem* 1992; **61**:897–946.
11. Cousins RJ. A role of zinc in the regulation of gene expression. *Proc Nutr Soc* 1998; **57**:307–311.
12. Kim AM, Vogt S, O'Halloran TV, Woodruff TK. Zinc availability regulates exit from meiosis in maturing mammalian oocytes. *Nat Chem Biol* 2010; **6**:674–681.
13. Bernhardt ML, Kim AM, O'Halloran TV, Woodruff TK. Zinc requirement during meiosis I-meiosis II transition in mouse oocytes is independent of the MOS-MAPK pathway. *Biol Reprod* 2011; **84**: 526–536.
14. Bernhardt ML, Kong BY, Kim AM, O'Halloran TV, Woodruff TK. A zinc-dependent mechanism regulates meiotic progression in mammalian oocytes. *Biol Reprod* 2012; **86**:114.
15. Kim AM, Bernhardt ML, Kong BY, Ahn RW, Vogt S, Woodruff TK, O'Halloran TV. Zinc sparks are triggered by fertilization and facilitate cell cycle resumption in mammalian eggs. *ACS Chem Biol* 2011; **6**:716–723.
16. Que EL, Duncan FE, Bayer AR, Philips SJ, Roth EW, Bleher R, Gleber SC, Vogt S, Woodruff TK, O'Halloran TV. Zinc sparks induce physiochemical changes in the egg zona pellucida that prevent polyspermy. *Integr Biol* 2017; **9**:135–144.
17. Hu Q, Duncan FE, Nowakowski AB, Antipova OA, Woodruff TK, O'Halloran TV, Wolfner MF. Zinc dynamics during drosophila oocyte maturation and egg activation. *iScience* 2020; **23**:101275.
18. Seeler J, Sharma A, Zaluzec NJ, Bleher R, Lai B, Schultz EG, Hoffman BM, LaBonne C, Woodruff TK, O'Halloran TV. Metal ion fluxes controlling amphibian fertilization. *Nat Chem* 2021; **13**: 683–691.
19. Duncan FE, Que EL, Zhang N, Feinberg EC, O'Halloran TV, Woodruff TK. The zinc spark is an inorganic signature of human egg activation. *Sci Rep* 2016; **6**:24737.
20. Kong BY, Duncan FE, Que EL, Kim AM, O'Halloran TV, Woodruff TK. Maternally-derived zinc transporters ZIP6 and ZIP10 drive the mammalian oocyte-to-egg transition. *Mol Hum Reprod* 2014; **20**:1077–1089.
21. Kong BY, Bernhardt ML, Kim AM, O'Halloran TV, Woodruff TK. Zinc maintains prophase I arrest in mouse oocytes through regulation of the MOS-MAPK pathway. *Biol Reprod* 2012; **87**: 11–12.
22. Kong BY, Duncan FE, Que EL, Xu Y, Vogt S, O'Halloran TV, Woodruff TK. The inorganic anatomy of the mammalian preimplantation embryo and the requirement of zinc during the first mitotic divisions. *Dev Dyn* 2015; **244**:935–947.
23. Que EL, Bleher R, Duncan FE, Kong BY, Gleber SC, Vogt S, Chen S, Garwin SA, Bayer AR, Dravid VP, Woodruff TK, O'Halloran TV. Quantitative mapping of zinc fluxes in the mammalian egg reveals the origin of fertilization-induced zinc sparks. *Nat Chem* 2015; **7**: 130–139.
24. Riddle, D. L., Blumenthal, T., Meyer, B. J., & Priess, J. R.. Introduction to *C. elegans*. In Riddle D. L., Blumenthal T., Meyer B. J., Priess J. R. (eds.), *C. elegans II*, 2nd ed.. Cold Spring Harbor NY: Cold Spring Harbor Laboratory Press; 1997. https://www.ncbi.nlm.nih.gov/pubmed/21413243.
25. Wignall SM, Villeneuve AM. Lateral microtubule bundles promote chromosome alignment during acentrosomal oocyte meiosis. *Nat Cell Biol* 2009; **11**:839–844.
26. Barton MK, Kimble J. *fog-1*, a regulatory gene required for specification of spermatogenesis in the germ line of Caenorhabditis elegans. *Genetics* 1990; **125**:29–39.
27. Roh HC, Collier S, Guthrie J, Robertson JD, Kornfeld K. Lysosome-related organelles in intestinal cells are a zinc storage site in *C. elegans*. *Cell Metab* 2012; **15**:88–99.
28. Stiernagle T. Maintenance of *C. elegans*. *WormBook* 2006; 1–11. https://doi.org/10.1895/wormbook.1.101.1.
29. Shaham S. Methods in cell biology. In: Ambros V. (ed.), *The C. elegans Research Community,* Worm Book; 2006. https://doi.org/doi/10.1895/wormbook.1.49.1 (5 February 2017, date last accessed).
30. Laband K, Lacroix B, Edwards F, Canman JC, Dumont J. Live imaging of *C. elegans* oocytes and early embryos. *Methods Cell Biol* 2018; **145**:217–236.
31. Vogt S. MAPS: a set of software tools for analysis and visualization of 3D X-ray fluorescence data sets. *J Phys IV* 2003; **104**: 635–638.
32. Roh HC, Collier S, Deshmukh K, Guthrie J, Robertson JD, Kornfeld K. Ttm-1 encodes CDF transporters that excrete zinc from intestinal cells of *C. elegans* and act in a parallel negative feedback circuit that promotes homeostasis. *PLoS Genet* 2013; **9**:e1003522.
33. Kim ESL, Sun L, Gabel CV, Fang-Yen C. Long-term imaging of *Caenorhabditis elegans* using nanoparticle-mediated immobilization. *PLoS One* 2013; **8**:e53419.
34. Schindelin J, Arganda-Carreras I, Frise E, Kaynig V, Longair M, Pietzsch T, Preibisch S, Rueden C, Saalfeld S, Schmid B, Tinevez

JY, White DJ, *et al*. Fiji: an open-source platform for biological-image analysis. *Nat Methods* 2012; **9**:676–682.
35. Schneider CA, Rasband WS, Eliceiri KW. NIH image to ImageJ: 25 years of image analysis. *Nat Methods* 2012; **9**:671–675. https://www.ncbi.nlm.nih.gov/pubmed/22930834.
36. Merzin M. *Applying stereological method in radiology. Volume measurement*. University of Tartu; 2008.
37. Frederickson C. Imaging zinc: old and new tools. *Sci STKE* 2003; **2003**:pe18. https://doi.org/10.1126/stke.2003.182.pe18.
38. Barton MK, Kimble J. Fog-1, a regulatory gene required for specification of spermatogenesis in the germ line of *Caenorhabditis elegans*. *Genetics* 1990; **125**:29–39.
39. Huelgas-Morales G, Greenstein D. Control of oocyte meiotic maturation in *C. elegans*. *Semin Cell Dev Biol* 2018; **84**: 90–99.
40. Mendoza AD, Woodruff TK, Wignall SM, O'Halloran TV. Zinc availability during germline development impacts embryo viability in *Caenorhabditis elegans*. *Comp Biochem Physiol C Toxicol Pharmacol* 2017; **191**:194–202.
41. Earley BJ, Mendoza AD, Tan CH, Kornfeld K. Zinc homeostasis and signaling in the roundworm *C. elegans*. *Biochim Biophys Acta Mol Cell Res* 2021; **1868**:118882.
42. Johnston WL, Dennis JW. The eggshell in the *C. elegans* oocyte-to-embryo transition. *Genesis* 2012; **50**:333–349.
43. Johnston WL, Krizus A, Dennis JW. The eggshell is required for meiotic fidelity, polar-body extrusion and polarization of the *C. elegans* embryo. *BMC Biol* 2006; **4**:35.
44. Johnston WL, Krizus A, Dennis JW. Eggshell chitin and chitin-interacting proteins prevent polyspermy in *C. elegans*. *Curr Biol* 2010; **20**:1932–1937.
45. Stein KK, Golden A. *The C. elegans eggshell*. WormBook 2015: 1–35. https://doi.org/10.1895/wormbook.1.179.1.
46. Hester J, Hanna-Rose W, Diaz F. Zinc deficiency reduces fertility in *C. elegans* hermaphrodites and disrupts oogenesis and meiotic progression. *Comp Biochem Physiol C Toxicol Pharmacol* 2017; **191**:203–209.
47. McCarter J, Bartlett B, Dang T, Schedl T. On the control of oocyte meiotic maturation and ovulation in *Caenorhabditis elegans*. *Dev Biol* 1999; **205**:111–128.
48. Bembenek JN, Richie CT, Squirrell JM, Campbell JM, Eliceriri KW, Poteryaev D, Spang A, Golden A, White JG. Cortical granule exocytosis in *C. elegans* is regulated by cell cycle components including separase. *Development* 2007; **134**:3837–3848.
49. Wozniak KL, Bainbridge RE, Summerville DW, Tembo M, Phelps WA, Sauer ML, Wisner BW, Czekalski ME, Pasumarthy S, Hanson ML, Linderman MB, Luu CH, *et al*. Zinc protection of fertilized eggs is an ancient feature of sexual reproduction in animals. *PLoS Biol* 2020; **18**:e3000811.